Implicit Eulerian Fluid-Structure Interaction Method for the Modeling of Highly Deformable Elastic Membranes

Aymen Laadhari, Gábor Székely

***Abstract*—**This paper is concerned with the development of a fully implicit and purely Eulerian fluid-structure interaction method tailored for the modeling of the large deformations of elastic membranes in a surrounding Newtonian fluid. We consider a simplified model for the mechanical properties of the membrane, in which the surface strain energy depends on the membrane stretching. The fully Eulerian description is based on the advection of a modified surface tension tensor, and the deformations of the membrane are tracked using a level set strategy. The resulting nonlinear problem is solved by a Newton-Raphson method, featuring a quadratic convergence behavior. A monolithic solver is implemented, and we report several numerical experiments aimed at model validation and illustrating the accuracy of the presented method. We show that stability is maintained for significantly larger time steps.

***Keywords*—**Fluid-membrane interaction, stretching, Eulerian, finite element method, Newton, implicit.

I. Introduction

THIS computational framework is concerned with the development and numerical implementation of a fully Eulerian methodology suitable for the modeling of the large deformations of elastic membranes in a surrounding Newtonian fluid. Such thin elastic structures, for which the membrane thickness is vanishingly small compared to the dimensions of the structure, are abundant in many biomedical and industrial applications, e.g. heart valves, capsules or red blood cells.

Heart valves are composed of thin, stiff but compliant flaps of tissue (called leaflets) attached to the heart wall. The leaflets open and close in a synchronised fashion to regulate blood flow and induce the periodic circulation of blood between the heart and the entire body. For the aortic valve, the leaflets thickness is about 0.5 mm, while the aorta diameter at the sinotubular junction is about 26 mm [5], [10], [17], [18]. Similarly, phospholipid membranes and capsules are thin elastic structures highly deformable that are found in nature (red blood cells, bacteria, etc.) and also they are widely used in biomedical, pharmaceutical and cosmetic applications. In particular, the membrane thickness of red blood cells is approximately about 5 nm, while the typical cell dimension is about 10 μm [32]. Red blood cells can withstand hydrodynamic stresses in the microcirculation and large arteries, due to their mechanical properties [3].

A. Laadhari is with the Department of Information Technology and Electrical Engineering, Swiss Federal Institute of Technology Zürich (Eidgenössische Technische Hochschule Zürich), CH-8092 Zürich, Switzerland (e-mail: laadhari@vision.ee.ethz.ch).

G. Székely is with the Department of Information Technology and Electrical Engineering, Swiss Federal Institute of Technology Zürich (Eidgenössische Technische Hochschule Zürich), CH-8092 Zürich, Switzerland.

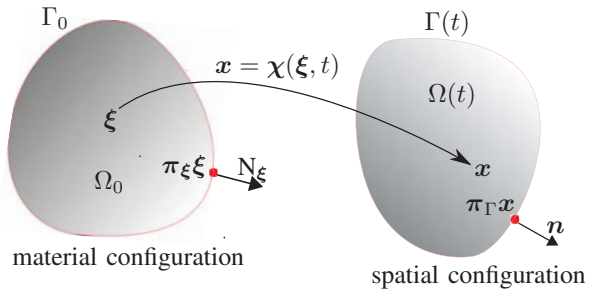

Fig. 1 A sketch for the elastic membrane in material (reference) and spatial (actual) configurations, and forward characteristics in Eulerian elasticity

To model the dynamics of such thin membranes under the influence of viscous forces induced by the surrounding fluid, several models and approaches have been developed in the literature, see e.g. [2], [5], [10], [11], [15], [22], [31]. Methodologies modeling the membrane mechanics can be roughly sorted according to the framework used to describe the structural problem: Lagrangian or Eulerian. Very briefly, Lagrangian methods rely on an explicit description of the motion and deformations of the elastic structure [11], [13], [22], [27], [29]. A mesh fits then the shape during the dynamics. Although the Lagrangian description of the motion and strain measures appears to be rather obvious, many numerical complexities can arise when studying large structural deformations. Eulerian approaches represent a promising alternative to readily handle contact issues and model large deformations, see [7], [8], [10], [15], [16], [19], [21], [33].

Regarding the numerical approximations, fully implicit, with respect to time, and monolithic approaches are barely used in the literature. The elasticity problem and the fluid problem are usually solved in a segregated manner, while the elastic force appears as a right hand side in the momentum equation. In general, the fully explicit decoupling strategies can lead to severe stability conditions when the problem is highly nonlinear, while the implicit time discretization methods help to overcome stability issues related to the time step restriction [14].

This mathematical framework consists in studying the mechanical interaction between the highly deformable elastic membrane and the surrounding fluid. We opt for describing

the phenomenon by a purely Eulerian description of motion, where the membrane is tracked using a level set approach. This setting allows a unified representation and a unique solver for the mechanics of the membrane and the fluid. In addition, a fully implicit time integration scheme is described and the derived system is solved using the Newton-Raphson method.

The paper is organized as follows: In Section II, we introduce some required notations and provide the mathematical formulation of the coupled nonlinear problem. Section III presents the semidiscrete finite element approximation and describes the tangent problem. A set of numerical examples showing the main features and the accuracy of the methodology are described in Section IV. The conclusions and forthcoming extensions are summarized in Section V. Details about the linearization procedure are provided in Appendix A.

II. Mathematical Setting

A. Notations

Let the symbols $\otimes$ and : denote the tensorial product and the two times contracted product between tensors, respectively. Let $\mathbf{n}$ denote the outward unit normal vector to a given surface Γ. We define the projector tensor $\boldsymbol{\pi}_\Gamma \equiv \mathbf{I} - \mathbf{n}\otimes\mathbf{n}$, where $\mathbf{I}$ is the identity tensor. Let ψ and $\mathbf{v}$ be a scalar and a vector field, respectively. The surface gradient and the surface divergence operators are given by:

$$\boldsymbol{\nabla}_s\psi = \boldsymbol{\pi}_\Gamma\,\boldsymbol{\nabla}\psi \quad \text{and} \quad \mathrm{div}_s\,\mathbf{v} = \mathrm{tr}(\boldsymbol{\nabla}_s\mathbf{v}) = \boldsymbol{\pi}_\Gamma : \boldsymbol{\nabla}\mathbf{v},$$

We denote the symmetric part of a given tensor $\boldsymbol{\tau}$ by $\mathbf{sym}(\boldsymbol{\tau}) = \boldsymbol{\tau} + \boldsymbol{\tau}^T$. The membrane and its surrounding space are embedded in a larger computational domain denoted by Λ. We denote by $\boldsymbol{\nu}$ the outward unit normal vector to the external boundary $\partial\Lambda$. In what follows, we present the mathematical setting for the three-dimensional problem.

B. Eulerian Description of the Membrane Mechanics

Let $T > 0$ represent the period of the computations. For any time $t \in (0,T)$, let $\Omega(t)$ design the interior domain enclosed by an elastic membrane Γ, and having a Lipschitz continuous boundary $\Gamma(t) = \partial\Omega(t)$, see Fig. 1. We assume that the membrane thickness is vanishingly small, so that the mechanical properties are solely given by the planar stretches. For all $t \in (0,T)$, we assume that $\Gamma(t)\cap\partial\Lambda = \emptyset$. From now, the explicit dependence of Ω and Γ from t will be understood.

At the initial time $t = 0$, the interior medium and the membrane coincide with the reference configuration, denoted by Ω_0 and Γ_0, respectively. For $t > 0$, a material point that was positioned at $\boldsymbol{\xi}$ in the reference configuration, is located at $\boldsymbol{x} = \boldsymbol{\chi}(\boldsymbol{\xi},t)$ in the current configuration, where $\boldsymbol{\chi} : \Omega_0\times(0,T) \to \Omega\times(0,T)$ is the smooth one-to-one deformation map.

The inverse map is $\boldsymbol{\xi} : \Omega\times(0,T) \to \Omega_0\times(0,T)$. By $\boldsymbol{d} = \boldsymbol{x} - \boldsymbol{\xi}$ we denote the displacements and its material derivative gives the velocity field $\boldsymbol{u} \equiv \dfrac{D\boldsymbol{d}}{Dt}$. The tensor rate of deformation is $\mathbf{D}(\boldsymbol{u}) = \mathbf{sym}(\boldsymbol{\nabla u})/2$, where the gradient is taken with respect to spatial coordinates and the superscript T denotes the usual transpose operation. Let $\boldsymbol{\nabla}_{\boldsymbol{\xi}}$ and $\boldsymbol{\nabla}$ be the material gradient and the gradient with respect to spatial coordinates, respectively. The identity expressing the forward map in terms of the inverse map reads $\boldsymbol{\chi}^{-1}(\boldsymbol{\chi}(\boldsymbol{\xi},t)) = \boldsymbol{\xi}$. That enables to express the deformation gradient tensor $\mathbf{F} = \boldsymbol{\nabla}_{\boldsymbol{\xi}}\boldsymbol{\chi} = \boldsymbol{\nabla}\boldsymbol{\xi}^{-1}$ in both Lagrangian and Eulerian frameworks, respectively.

For an hyperelastic body, the hyperelastic strain energy potential expresses in terms of $\mathbf{F}$, typically treated in a Lagrangian formulation. However, an Eulerian description requires to formulate the solid mechanics in the same actual frame of reference as the fluid problem. When the thickness is vanishingly small, the membrane theory should be reformulated, yielding the Gurtin-Murdoch surface elasticity theory [12], [22]. To keep track of the position of material points on the membrane, we introduce the outward pointing normals on the membrane $\mathbf{N}_{\boldsymbol{\xi}}$ and $\mathbf{n}$ in the reference and actual configurations, respectively. From now, the surface projector on both configurations are denoted by

$$\boldsymbol{\pi}_\Gamma = \mathbf{I} - \mathbf{n}\otimes\mathbf{n} \quad \text{and} \quad \boldsymbol{\pi}_{\boldsymbol{\xi}} = \mathbf{I} - \mathbf{N}_{\boldsymbol{\xi}}\otimes\mathbf{N}_{\boldsymbol{\xi}}.$$

They project any material points on Γ_0 and $\Gamma(t)$, respectively (see sketch in Fig. 1).

The surface deformation gradient $\mathbf{F}_s$ only considers the in-plane deformations of $\boldsymbol{\nabla}_{\boldsymbol{\xi}}\boldsymbol{x}$ in the tangential plane, yielding $\mathbf{F}_s = \boldsymbol{\pi}_\Gamma\mathbf{F}\boldsymbol{\pi}_{\boldsymbol{\xi}}$ [22]. Both $\mathbf{F}_s$ and $\mathbf{F}$ have the same dimension. It follows that $\mathbf{F}_s.\mathbf{N}_{\boldsymbol{\xi}} = \mathbf{0}$, and $\mathbf{F}_s$ is consequently rank deficient with zero eigenvalue corresponding to the eigenvector $\mathbf{N}_{\boldsymbol{\xi}}$. The left Cauchy-Green surface strain tensor $\mathbf{B}_s$ is expressed with respect to the stretch tensor $\boldsymbol{\Lambda}$ such that

$$\mathbf{B}_s = \boldsymbol{\Lambda}^2 = \mathbf{F}_s\mathbf{F}_s^T = \boldsymbol{\pi}_\Gamma\mathbf{T}_s\boldsymbol{\pi}_\Gamma \quad \text{with} \quad \mathbf{T}_s = \mathbf{F}\boldsymbol{\pi}_{\boldsymbol{\xi}}\mathbf{F}^T. \quad (1)$$

The eigenvalues λ_1, λ_2 of the stretch tensor $\boldsymbol{\Lambda}$ represent the principle planar stretches in the tangent plane of the membrane Γ. From the eigenvalues, the surface strain invariants can be introduced as:

$$J_s \equiv \lambda_1\lambda_2 = \sqrt{\frac{1}{2}\Big((\mathrm{tr}\,\mathbf{B}_s)^2 - \mathrm{tr}\,(\mathbf{B}_s^2)\Big)} \quad \text{and}$$
$$I_s \equiv \frac{\lambda_1^2+\lambda_2^2}{2} - 1 = \frac{1}{2}\,\mathrm{tr}\,\mathbf{B}_s - 1.$$

In particular, J_s represents the local membrane area change and enables to express the ratio of the deformed to the undeformed surface area between the two configurations [22].

For a hyperelastic membrane, the surface strain energy function is expressed with respect to the surface tensor $\mathbf{F}_s$ and then in terms of its invariants. In the present work, we consider a simplified constitutive law, in which the surface strain energy only depends on the membrane stretching [33]. We assume that:

$$\mathcal{W}(\mathbf{F}_s) = \mathcal{W}(J_s).$$

Nevertheless, we emphasize that we aim to present a methodology that can be easily extended to model the entire mechanical response, i.e. depending on both invariants J_s and I_s. Therefore, the surface Cauchy-Green stress tensor $\boldsymbol{\sigma}_s$ can be expressed in terms of the first surface Piola Kirchhoff

stress tensor. Let us introduce the inverse surface deformation gradient $\hat{\mathbf{F}}_s \equiv \boldsymbol{\nabla}\boldsymbol{\xi}$. It follows from

$$\frac{\partial J_s}{\partial \mathbf{F}_s} = J_s \hat{\mathbf{F}}_s$$

and the identity satisfied by the surface deformation gradient tensor: $\mathbf{F}_s\hat{\mathbf{F}}_s = \boldsymbol{\pi}_\Gamma$ that

$$\boldsymbol{\sigma}_s = \frac{1}{J_s}\frac{\partial \mathcal{W}}{\partial \mathbf{F}_s}.\mathbf{F}_s^T = \frac{1}{J_s}\frac{\partial \mathcal{W}}{\partial J_s}\frac{\partial J_s}{\partial \mathbf{F}_s}.\mathbf{F}_s^T = \mathcal{W}'\left(J_s\right)\boldsymbol{\pi}_\Gamma.$$

Hence, the elastic force exerted by the membrane reads:

$$\mathcal{F}_\Gamma = \mathbf{div}_s\,\boldsymbol{\sigma}_s = \boldsymbol{\nabla}_s\mathcal{W}'\big(\exp I_1^s\big) - \mathcal{W}'\big(\exp I_1^s\big)\,\mathrm{div}_s\,\mathbf{n}\,\mathbf{n}.$$

That corresponds to the same expression obtained in [33].

To achieve a purely Eulerian description of the membrane mechanics, we need to recover the deformation history on the membrane. To that end, it follows from the following expressions of the material derivatives:

$$\frac{D\mathbf{F}}{Dt} = \boldsymbol{\nabla}\boldsymbol{u}\,\mathbf{F} \qquad \text{and} \qquad \frac{D\boldsymbol{\pi}_\xi}{Dt} = \mathbf{0}$$

together with the expression of $\mathbf{T}_s$ (1) that

$$\frac{\partial \mathbf{T}_s}{\partial t} + \boldsymbol{u}\cdot\boldsymbol{\nabla}\mathbf{T}_s = \mathbf{sym}\left(\boldsymbol{\nabla}\boldsymbol{u}\,\mathbf{T}_s\right). \tag{2}$$

The previous equation is fully Eulerian and enables to describe the mechanical response of the membrane. Remark that, in this simplified elasticity model, it would be easier to consider the advection of the invariant J_s instead of $\mathbf{T}_s$ (2). However, as we aim to describe a general framework that can be easily extended to the full elastic response (i.e. the surface strain energy function relies on both strain invariants), we opt to advect $\mathbf{T}_s$. In such a case, the strain invariants can always be deduced from the tensor $\mathbf{T}_s$.

From now, $\Omega(t)$, $t \geqslant 0$ stands for the interior fluid domain enclosed by Γ.

C. Level Set Method

The membrane Γ is described implicitly as the zero level set of a function φ [25]:

$$\Gamma(t) = \Big\{(t,\boldsymbol{x}) \in (0,T)\times\Lambda : \varphi(t,\boldsymbol{x}) = 0\Big\}.$$

For any $t \in (0,T)$, a time-dependent initial value partial differential equation describes the motion of Γ:

$$\frac{\partial \varphi}{\partial t} + \boldsymbol{u}\cdot\boldsymbol{\nabla}\varphi = 0, \quad \text{in } (0,T)\times\Lambda. \tag{3}$$

This problem is initialized with a suitable distance function φ_0 to $\Gamma(0)$:

$$\varphi_0(\boldsymbol{x}) = \begin{cases} \inf\limits_{\boldsymbol{y}\in\Gamma(0)} |\boldsymbol{y}-\boldsymbol{x}| & \text{if } \boldsymbol{x}\notin\Omega(0), \\ -\inf\limits_{\boldsymbol{y}\in\Gamma(0)} |\boldsymbol{y}-\boldsymbol{x}| & \text{otherwise.}\end{cases}$$

This equation is equipped with suitable boundary and initial data:

$$\varphi = \varphi_b \text{ on } (0,T)\times\Sigma_- \quad \text{and} \quad \varphi(0) = \varphi_0 \text{ in } \Lambda,$$

where $\Sigma_- = \big\{\boldsymbol{x}\in\partial\Lambda : \mathbf{v}\cdot\boldsymbol{\nu}(\boldsymbol{x}) < 0\big\}$ represents the upstream boundary. Geometrical quantities such as the normal $\mathbf{n}$ and mean cuvature H are extended to the entire Λ and are easily recovered implicitly in terms of the level set φ:

$$\mathbf{n} = \frac{\boldsymbol{\nabla}\varphi}{|\boldsymbol{\nabla}\varphi|} \qquad \text{and} \qquad H = \mathrm{div}_s\,\mathbf{n} = \mathrm{div}\,\mathbf{n}.$$

A regularization approach is commonly introduced to avoid using meshes that follow the membrane deformations. Let us introduce a regularization parameter ε proportional to the mesh size h. The regularized Heaviside function $\mathscr{H}$, Dirac measure δ_Γ and sign function sgn in a banded strip of width 2ε are given by:

$$\mathscr{H}_\varepsilon(\varphi) = \begin{cases} 0, & \text{when } \varphi < -\varepsilon \\ \dfrac{1}{2}\left(1 + \dfrac{\varphi}{\varepsilon} + \dfrac{1}{\pi}\sin\left(\dfrac{\pi\varphi}{\varepsilon}\right)\right), & \text{when } |\varphi| \leqslant \varepsilon, \\ 1, & \text{otherwise}\end{cases}$$

$$\delta_\varepsilon(\varphi) = \frac{\mathrm{d}\mathscr{H}_\varepsilon}{\mathrm{d}\varphi}(\varphi) \quad \text{and} \quad \mathrm{sgn}_\varepsilon(\varphi) = 2\mathscr{H}_\varepsilon(\varphi) - 1.$$

For any given function $\eta(\cdot)$ defined on Γ, an extension $\tilde{\eta}(\cdot)$ to Λ is required, and the surface integrals are approximated by:

$$\int_\Gamma \eta(\boldsymbol{x})\; d\boldsymbol{s} = \int_\Lambda |\nabla\varphi|\;\delta_\Gamma\,\tilde{\eta}(\boldsymbol{x})\,d\boldsymbol{x} \approx \int_\Lambda |\nabla\varphi|\;\delta_\varepsilon\left(\varphi\right)\;\tilde{\eta}(\boldsymbol{x})\,d\boldsymbol{x}.$$

The advection of the level set function degenerates the initial signed distance property. The gradient norm may vanish or blow up and singularities can arise. This issue is circumvented by solving an auxiliary redistancing problem [25] that helps to reestablish the initial signed distance behavior. A modified version of the classical redistancing problem has been used here, where an explicit Lagrange multiplier acts as a constraint enforcing the unphysical shifting of the membrane during the redistancing process [20]. For $t \in (0,T)$, we introduce a pseudo-time variable τ and we search for a quasi-stationary solution ϕ of the penalized redistancing problem:

$$\begin{aligned}\partial_\tau\phi(\tau,\cdot;t) + \hat{\mathbf{v}}\cdot\nabla\phi(\tau,\cdot;t) &= \mathrm{sgn}_\varepsilon(\varphi(t,\cdot)) \\ &\quad + \lambda(\tau,\cdot;t)g_\varepsilon(\phi(\tau,\cdot;t)), \\ \phi(0,\cdot;t) &= \varphi(t,\cdot),\end{aligned}$$

where $\varphi(t,\cdot)$ is the solution of (3) and the advection field is $\hat{\mathbf{v}} = \mathrm{sgn}_\varepsilon(\varphi)\nabla\phi/\,|\nabla\phi|$. The forcing term $\lambda(\tau,\boldsymbol{x};t)$ imposes the constraint of local mass preservation at $\boldsymbol{x}\in\Lambda$, and the function $g_\varepsilon(\phi)$ acts in the vicinity of the membrane, see a detailed description in [20]. The level set is subsequently updated with the quasi-stationary solution of the auxiliary redistancing problem, and approximates a signed distance function. At the numerical level, we use a first order combined characteristic and finite difference discretization method to approximate the advection term in the redistancing problem. We also consider the Gauss-Lobatto quadrature formula which guarantees further stability for the characteristics method [6], [30].

D. Statement of the Nonlinear Coupled Problem

Let us consider a Newtonian fluid in both sides of the membrane Γ. We assume constant density ρ and dynamic viscosity μ of the fluid inside and outside the membrane.

Let $\boldsymbol{\sigma}(\boldsymbol{u},p) = 2\mu\mathbf{D}(\boldsymbol{u}) - p\boldsymbol{I}$ be the fluid Cauchy stress tensor. We consider two complementary subsets Σ_D and Σ_N of the boundary $\partial\Lambda$ on which essential or natural boundary conditions are assigned, respectively. Let $\boldsymbol{u}_b$ represent a fixed velocity field on Σ_D.

Let us denote by $[\boldsymbol{u}]_-^+ = \boldsymbol{u}_+ - \boldsymbol{u}_-$ and $[\boldsymbol{\sigma}\mathbf{n}]_-^+ = \boldsymbol{\sigma}_+\mathbf{n} - \boldsymbol{\sigma}_-\mathbf{n}$ the jumps in the velocity and normal stress across the membrane, respectively. It follows from the differential balance of the hydrodynamic and elastic forces on an infinitesimal domain on the membrane that $[\boldsymbol{\sigma}\mathbf{n}]_-^+ = -\mathcal{F}_\Gamma$.

Collecting the elements above, we end with the following coupled model describing the Eulerian fluid-membrane interaction problem: $\mathscr{P}$: *find the velocity* $\boldsymbol{u}$*, pressure* p*, surface tensor* $\mathbf{T}_s$ *and level set function* φ *such that*

$$
\begin{aligned}
\rho\left(\frac{\partial \boldsymbol{u}}{\partial t} + \boldsymbol{u}.\nabla\boldsymbol{u}\right) - \mathbf{div}\,\boldsymbol{\sigma}(\boldsymbol{u},p,\varphi) &= \rho\boldsymbol{g} \ \text{ in } (0,T)\times(\Lambda\backslash\Gamma)\\
\text{div } \boldsymbol{u} &= 0 \quad \text{ in } (0,T)\times\Lambda\\
[\boldsymbol{u}]_-^+ &= \mathbf{0} \quad \text{ on } (0,T)\times\Gamma\\
[\boldsymbol{\sigma}\mathbf{n}]_-^+ &= -\,\mathbf{div}_s\,\boldsymbol{\sigma}_s \quad \text{ on } (0,T)\times\Gamma\\
\frac{\partial \mathbf{T}_s}{\partial t} + \boldsymbol{u}\cdot\boldsymbol{\nabla}\mathbf{T}_s &= \mathbf{sym}\left(\boldsymbol{\nabla}\boldsymbol{u}\,\mathbf{T}_s\right) \quad \text{ on } (0,T)\times\Lambda\\
\frac{\partial \varphi}{\partial t} + \boldsymbol{u}.\nabla\varphi &= 0 \quad \text{ in } (0,T)\times\Lambda\\
\varphi &= \varphi_b, \ \text{ on } \quad (0,T)\times\Sigma_-\\
\boldsymbol{u} &= \boldsymbol{u}_b, \ \text{ on } \quad (0,T)\times\Sigma_D\\
\boldsymbol{\sigma}\boldsymbol{\nu} &= \mathbf{0} \quad \text{ on } \ (0,T)\times\Sigma_N.
\end{aligned}
$$

The system is endowed with initial data which are given by $\boldsymbol{u}(0) = \boldsymbol{u}_0$, $\varphi(0) = \varphi_0$ and $\mathbf{T}_s(0) = \mathbf{T}_{s,0}$. We assume that the membrane shape Γ is sufficiently regular during the dynamics. The normal stress discontinuity across the membrane leads to a singular elastic force in the momentum equation.

III. Finite Element Approximation

The present method has been implemented using the C++ library for scientific computing Rheolef [30]. Distributed-memory parallelism relies on MPI [23]. The package Mumps [1], [24] is used for the factorization and as direct solver on distributed memory architectures. Numerical results are displayed graphically using the softwares Paraview [26] and Gnuplot [36].

A. Time Discretization

Let us divide $[0,T]$ into N subintervals $[t^n, t^{n+1})$, $n = 0,\ldots,N-1$ of uniform time steps Δt. For any $n \geqslant 1$, the unknowns $\boldsymbol{u}^n$, p^n, $\mathbf{T}_s^n$ and φ^n at time step n are computed iteratively. The surface projector is approximated at t^n by $\boldsymbol{\pi}_\Gamma^n = \mathbf{I} - \mathbf{n}^n \otimes \mathbf{n}^n$. Accordingly, the surface operators div_s^n and $\boldsymbol{\nabla}_s^n$ are approximated at time t^n.

To write the variational formulation, the problem $\mathscr{P}$ is tested with suitable test functions and we shall integrate the momentum equation in both Ω and $\Lambda\backslash\overline{\Omega}$ separately. It follows from the Green formulation adapted for surface integrals that:

$$
\begin{aligned}
\int_\Gamma \mathrm{div}_s\,\boldsymbol{\sigma}_s\cdot\mathbf{v} &= \int_\Gamma H\,(\boldsymbol{\sigma}_s\mathbf{n})\cdot\mathbf{v} - \int_\Gamma \boldsymbol{\sigma}_s : \boldsymbol{\nabla}_s\mathbf{v} + \int_{\partial\Gamma}(\boldsymbol{\sigma}_s\boldsymbol{\nu})\cdot\mathbf{v}\\
&= \int_\Gamma \mathcal{W}'\,(J_s)\,\boldsymbol{\pi}_\Gamma : \boldsymbol{\nabla}_s\mathbf{v},
\end{aligned}
$$

resulting from the assumption of a closed membrane. We introduce the functional spaces of admissible velocities, pressures, membrane tension and level set function:

$$
\begin{aligned}
&\mathbb{V}(\boldsymbol{u}_b) = \left\{\mathbf{v}\in\left(H^1(\Lambda)\right)^d \ :\ \mathbf{v} = \boldsymbol{u}_b \ \text{ on } \Sigma_D\right\},\\
&\mathbb{Q} = \left\{q\in L^2(\Lambda) : \int_\Lambda q\,d\boldsymbol{x} = 0\right\},\\
&\mathbb{W} = \left\{\boldsymbol{\tau}\in\left(L^2(\Lambda)\right)^{d\times d} : \boldsymbol{\tau} = \boldsymbol{\tau}^T\right\}\\
&\text{and } \ \mathbb{X}(\varphi_b) = \left\{\psi\in W^{1,\infty}(\Lambda) \ :\ \psi = \varphi_b \ \text{ on } \Sigma_-\right\}.
\end{aligned}
$$

The semi-discretized problem $\mathscr{P}$ reads:

find $\boldsymbol{\chi} \equiv (\boldsymbol{u}^n, p^n, \mathbf{T}_s^n, \varphi^n) \in \mathbb{V}(\boldsymbol{u}_b)\times\mathbb{Q}\times\mathbb{W}\times\mathbb{X}(\varphi^{n-1})$ *such that*

$$
\begin{aligned}
&\int_\Lambda \rho\left(\frac{\boldsymbol{u}^n - \boldsymbol{u}^{n-1}}{\Delta t} + \boldsymbol{u}^n\cdot\boldsymbol{\nabla}\boldsymbol{u}^n\right)\cdot\mathbf{v} + \int_\Lambda 2\mu\mathbf{D}\,(\boldsymbol{u}^n) : \mathbf{D}(\mathbf{v})\\
&\quad + \int_\Lambda \delta_\varepsilon\,(\varphi^n)\,|\boldsymbol{\nabla}\varphi^n|\,\mathcal{W}'\,(J_s^n)\left(\mathbf{I} - \frac{\boldsymbol{\nabla}\varphi^n}{|\boldsymbol{\nabla}\varphi^n|}\otimes\frac{\boldsymbol{\nabla}\varphi^n}{|\boldsymbol{\nabla}\varphi^n|}\right) : \boldsymbol{\nabla}\mathbf{v}\\
&\quad - \int_\Lambda p^n\,\mathrm{div}\ \mathbf{v} = \int_\Lambda \rho\,\boldsymbol{g}\cdot\mathbf{v}, \qquad (4)\\
&\int_\Lambda q\ \mathrm{div}\ \boldsymbol{u}^n = 0, \qquad (5)\\
&\int_\Lambda \frac{\mathbf{T}_s^n - \mathbf{T}_s^{n-1}}{\Delta t} : \boldsymbol{\tau} + \int_\Lambda (\boldsymbol{u}^n\cdot\nabla\mathbf{T}_s^n) : \boldsymbol{\tau}\\
&\quad - \int_\Lambda \mathbf{sym}\,(\boldsymbol{\nabla}\boldsymbol{u}^n\mathbf{T}_s^n) : \boldsymbol{\tau} = 0, \qquad (6)\\
&\int_\Lambda \frac{\varphi^n - \varphi^{n-1}}{\Delta t}\psi + \int_\Lambda (\boldsymbol{u}^n\cdot\nabla\varphi^n)\,\psi = 0, \qquad (7)
\end{aligned}
$$

defined for all $\mathbf{v}\in\mathbb{V}(0)$, $q\in\mathbb{Q}$, $\boldsymbol{\tau}\in\mathbb{W}$ and $\psi\in\mathbb{X}\,(0)$.

Let us denote by $\boldsymbol{\chi}$ the global vector of unknowns $(\boldsymbol{u},p,\lambda,\varphi)$, and let $\Psi = (\mathbf{v},q,\xi,\psi)$ be the corresponding vector of test functions. All surface integrals in $\mathscr{P}^n$ are transformed into integrals over Λ as aforementioned in Section II-C. Let $\mathscr{R}\,(\boldsymbol{\chi})$ be the global residual vector corresponding to the regularized problem. Let $\langle .,.\rangle$ stand for the duality product. The problem (4-5-6-7) reads in a compact form:

find the unknowns $\boldsymbol{\chi}^n$ *such that*

$$
\begin{aligned}
&\Big\langle\mathscr{R}\,(\boldsymbol{\chi}^n)\,,\Psi\Big\rangle \equiv \Big(\big\langle\mathscr{R}_{\boldsymbol{\chi}}\,(\boldsymbol{\chi}^n)\,,\mathbf{v}\big\rangle_{\mathbb{V}(0)',\mathbb{V}(0)}, \big\langle\mathscr{R}_p(\boldsymbol{u}^n),q\big\rangle_{\mathbb{Q}',\mathbb{Q}},\\
&\big\langle\mathscr{R}_{\mathbf{T}_s}(\boldsymbol{u}^n,\mathbf{T}_s^n),\xi\big\rangle_{\mathbb{W}',\mathbb{W}}, \big\langle\mathscr{R}_{\boldsymbol{u},\varphi}(\boldsymbol{u}^n,\varphi^n),\psi\big\rangle_{\mathbb{X}(0)',\mathbb{X}(0)}\Big)^T = \mathbf{0}, \ \forall\Psi.
\end{aligned}
$$

B. Consistent Linearization and Newton Algorithm

Let $D\mathscr{R}\,(\boldsymbol{\chi})\,[\delta\boldsymbol{\chi}]$ represent the directional derivative of $\mathscr{R}$ in the direction $\delta\boldsymbol{\chi}$. The Newton-Raphson method reduces the nonlinear problem $\mathscr{R}\,(\boldsymbol{\chi}^n) = \mathbf{0}$ (4-5-6-7) into a sequence of

linear sub-problems [28]. Given the starting value $\boldsymbol{\chi}_0^n = \boldsymbol{\chi}^n$, the strategy consists in computing iteratively the solution $\boldsymbol{\chi}_k^n$ with $k > 0$. We search the velocity, pressure, surface tension and level set increments $\delta\boldsymbol{\chi}_k^n = (\delta\boldsymbol{u}_k^n; \delta p_k^n, \delta\lambda_k^n, \delta\varphi_k^n)$ at each sub-iteration $k \geqslant 1$ in such a way that

$$\Big\langle D\mathscr{R}\left(\boldsymbol{\chi}_k^n\right)\left[\delta\boldsymbol{\chi}_k^n\right], \mathbf{v}\Big\rangle = -\Big\langle \mathscr{R}\left(\boldsymbol{\chi}_k^n\right), \mathbf{v}\Big\rangle. \tag{8}$$

The solution is subsequantly updated by

$$\boldsymbol{\chi}_{k+1}^n = \boldsymbol{\chi}_k^n + \delta\boldsymbol{\chi}_k^n. \tag{9}$$

The Newton method is known to have local convergence properties, which means that the starting value needs to be close enough to the expected solution in order to ensure the convergence. For that reason, we use a second order extrapolation of the solution at the previous time steps to assign the initial guess $\boldsymbol{\chi}_0^n$. We apply recursively the algorithm and the stopping criterion is based on the computation of the global residual. We set the Newton tolerance to $\epsilon = 10^{-8}$. Note that one can use an inexact version of the Newton method, that consists in computing the tangent problem based on some simplifying assumptions. For instance, we can assume that the signed distance property is always achieved, due to the resolution of the redistancing problem until reaching the convergence. However, the quadratic convergence of the Newton algorithm can be drastically deteriorated if the signed distance property is not respected. In this work, we derive the exact tangent problem for a general level set function.

In what follows, we will drop the superscript n whenever it is clear from the context, and we rather write k as a superscript. To write the derived problem in a compact manner and to allow a straightforward finite element implementation, we introduce the following multi-linear forms:

$$\begin{aligned}
&a(\boldsymbol{u},\mathbf{v}) = \int_\Lambda 2\mathbf{D}(\boldsymbol{u}) : \mathbf{D}(\mathbf{v}); \quad b(\boldsymbol{u},q) = -\int_\Lambda q \operatorname{div}\boldsymbol{u};\\
&c(\boldsymbol{u},\mathbf{v};\boldsymbol{w}) = \int_\Lambda \left(\left(\boldsymbol{u}\cdot\boldsymbol{\nabla}\right)\boldsymbol{w} + \left(\boldsymbol{w}\cdot\boldsymbol{\nabla}\right)\boldsymbol{u}\right).\mathbf{v};\\
&d(\varphi,\mathbf{v};\boldsymbol{w},\mathbf{P}) = \int_\Lambda \left(\boldsymbol{w}\cdot\boldsymbol{\nabla}\varphi\right)\left(\mathbf{P} : \boldsymbol{\nabla}\mathbf{v}\right); \quad g(\boldsymbol{\tau},\mathbf{T}) = \int_\Lambda \boldsymbol{\tau} : \mathbf{T};\\
&f(\boldsymbol{\tau},\mathbf{v};\bar{\mathbf{P}},\mathbf{P}) = \int_\Lambda \left(\boldsymbol{\tau} : \bar{\mathbf{P}}\right)\left(\mathbf{P} : \boldsymbol{\nabla}\mathbf{v}\right); \quad m(\boldsymbol{u},\mathbf{v}) = \int_\Lambda \boldsymbol{u}\cdot\mathbf{v};\\
&h(\varphi,\psi;w) = \int_\Lambda w\,\varphi\psi; \quad i(\varphi,\psi;\boldsymbol{w}) = \int_\Lambda \psi\boldsymbol{w}\cdot\boldsymbol{\nabla}\varphi;\\
&j(\varphi,\boldsymbol{u};\boldsymbol{w}) = \int_\Lambda \varphi\boldsymbol{u}\cdot\boldsymbol{w}; \quad s(\varphi,\mathbf{v};\mathbf{P}) = \int_\Lambda \varphi\mathbf{P} : \boldsymbol{\nabla}\mathbf{v};\\
&\alpha(\boldsymbol{\tau},\mathbf{T};\boldsymbol{u}) = \int_\Lambda \left(\boldsymbol{u}\cdot\boldsymbol{\nabla}\boldsymbol{\tau} - \mathbf{sym}\left(\boldsymbol{\nabla}\boldsymbol{u}\,\boldsymbol{\tau}\right)\right) : \mathbf{T};\\
&\beta(\boldsymbol{u},\mathbf{T};\mathbf{P}) = \alpha(\mathbf{P},\mathbf{T};\boldsymbol{u});\\
&l(\varphi,\mathbf{v};w,\boldsymbol{w},\mathbf{P}) = \int_\Lambda w\Big(\left(\mathbf{P}\boldsymbol{\nabla}\varphi\right)\otimes\boldsymbol{w} + \boldsymbol{w}\otimes\left(\mathbf{P}\boldsymbol{\nabla}\varphi\right)\Big) : \boldsymbol{\nabla}\mathbf{v};\\
&\gamma(\varphi,\mathbf{v};\boldsymbol{w},\mathbf{P},\bar{\mathbf{P}}) = \int_\Lambda \left(\mathbf{P} : \boldsymbol{\nabla}\mathbf{v}\right)\\
&\qquad\qquad \bar{\mathbf{P}} : \Big(\left(\mathbf{P}\boldsymbol{\nabla}\varphi\right)\otimes\boldsymbol{w} + \boldsymbol{w}\otimes\left(\mathbf{P}\boldsymbol{\nabla}\varphi\right)\Big);
\end{aligned}$$

defined for all $\boldsymbol{u},\mathbf{v} \in \mathbb{V}$; $q \in \mathbb{Q}$; $\boldsymbol{\tau},\mathbf{T} \in \mathbb{W}$; $\varphi,\psi \in \mathbb{X}$; $w,\boldsymbol{w}_i,\mathbf{P}_{i,j},\bar{\mathbf{P}}_{i,j} \in L^\infty(\Lambda)$ with $1 \leqslant i,j \leqslant d$.

The residuals of the coupled system (4-5-6-7) are given, respectively, in a compact form by:

$$\begin{aligned}
\langle\mathscr{R}_{\boldsymbol{\chi}}\left(\boldsymbol{\chi}^k\right),\mathbf{v}\rangle &= \frac{\rho}{\Delta t}m\Big(\boldsymbol{u}^k - \boldsymbol{u}^{n-1},\mathbf{v}\Big) + \frac{\rho}{2}c\Big(\boldsymbol{u}^k,\mathbf{v};\boldsymbol{u}^k\Big)\\
&\quad + \mu a\Big(\boldsymbol{u}^k,\mathbf{v}\Big) + b\Big(\mathbf{v},p^k\Big) - \rho\, m\left(\boldsymbol{g},\mathbf{v}\right)\\
&\quad + s\Big(\delta_\varepsilon\left(\varphi^n\right)\left|\boldsymbol{\nabla}\varphi^n\right|\mathcal{W}'\left(J_s^n\right),\mathbf{v};\boldsymbol{\pi}_\Gamma^k\Big) \qquad (10)\\
\langle\mathscr{R}_p\left(\boldsymbol{u}^k\right),q\rangle &= b\Big(\boldsymbol{u}^k,q\Big), \qquad (11)\\
\langle\mathscr{R}_{\mathbf{T}_s}(\boldsymbol{u}^k,\mathbf{T}_s^k),\boldsymbol{\tau}\rangle &= \alpha\Big(\mathbf{T}_s^k,\boldsymbol{\tau};\boldsymbol{u}^k\Big)\\
&\quad + \frac{1}{\Delta t}g\left(\mathbf{T}_s^k - \mathbf{T}_s^{n-1},\boldsymbol{\tau}\right), \qquad (12)\\
\langle\mathscr{R}_\varphi\left(\varphi^k,\boldsymbol{u}^k\right),\psi\rangle_{\mathbb{X}(0)',\mathbb{X}(0)} &= \frac{1}{\Delta t}h\left(\varphi^k - \varphi^{n-1},\psi;1\right)\\
&\quad + i\left(\varphi^k,\psi;\boldsymbol{u}^k\right), \quad \forall\psi \in \mathbb{X}(0). \qquad (13)
\end{aligned}$$

For ease of exposition, the details on the linearization procedure are provided in Appendix A. The tangent problem corresponding to the coupled system (4-5-6-7) expresses in a compact form as:

given $\boldsymbol{\chi}^k$, *find* $\delta\boldsymbol{\chi}^k \equiv \left(\delta\boldsymbol{u}^k,\delta p^k,\delta\mathbf{T}_s^k,\delta\varphi^k\right) \in \mathbb{V}(\boldsymbol{u}_b)\times\mathbb{Q}\times\mathbb{W}\times\mathbb{X}(\varphi^{n-1})$ *such that*

$$\begin{aligned}
&\frac{\rho}{\Delta t}m\Big(\delta\boldsymbol{u}^k,\mathbf{v}\Big) + \rho c\Big(\delta\boldsymbol{u}^k,\mathbf{v};\boldsymbol{u}^k\Big) + \mu a\Big(\delta\boldsymbol{u}^k,\mathbf{v}\Big)\\
&\quad + s\Big(\delta\varphi^k,\mathbf{v};\delta_\varepsilon'\left(\varphi^k\right)\left|\boldsymbol{\nabla}\varphi^k\right|\mathcal{W}'\left(J_s^k\right)\boldsymbol{\pi}_\Gamma^k\Big)\\
&\quad + d\left(\delta\varphi^k,\mathbf{v};\delta_\varepsilon\left(\varphi^k\right)\mathcal{W}'\left(J_s^k\right)\frac{\boldsymbol{\nabla}\varphi^k}{|\boldsymbol{\nabla}\varphi^k|},\boldsymbol{\pi}_\Gamma^k\right)\\
&\quad - l\left(\delta\varphi^k,\mathbf{v};\delta_\varepsilon\left(\varphi^k\right)\mathcal{W}'\left(J_s^k\right),\frac{\boldsymbol{\nabla}\varphi^k}{|\boldsymbol{\nabla}\varphi^k|},\boldsymbol{\pi}_\Gamma^k\right)\\
&\quad + f\left(\delta\mathbf{T}_s^k,\mathbf{v};\left|\boldsymbol{\nabla}\varphi^k\right|\mathcal{W}''\left(J_s^k\right)\frac{\delta_\varepsilon\left(\varphi^k\right)}{2J_s^k}\right.\\
&\qquad\qquad \left.\Big(\left(\mathbf{T}_s^k : \boldsymbol{\pi}_\Gamma^k\right)\mathbf{I} - \mathbf{T}_s^k\boldsymbol{\pi}_\Gamma^k\Big)\boldsymbol{\pi}_\Gamma^k,\boldsymbol{\pi}_\Gamma^k\right)\\
&\quad + \gamma\left(\delta\varphi^k,\mathbf{v};\boldsymbol{\nabla}\varphi^k,\boldsymbol{\pi}_\Gamma^k,\mathcal{W}''\left(J_s^k\right)\frac{\delta_\varepsilon\left(\varphi^k\right)}{2J_s^k\left|\boldsymbol{\nabla}\varphi^k\right|}\right.\\
&\qquad\qquad \left.\Big(\mathbf{T}_s^k\mathbf{P}^k\mathbf{T}_s^k - \left(\mathbf{T}_s^k : \mathbf{P}^k\right)\mathbf{T}_s^k\Big)\right)\\
&\quad + b\Big(\mathbf{v},\delta p^k\Big) = -\Big\langle\mathscr{R}_{\boldsymbol{\chi}}\left(\boldsymbol{\chi}^k\right),\mathbf{v}\Big\rangle_{\mathbb{V}(\mathbf{0})',\mathbb{V}(\mathbf{0})}, \qquad (14)\\
&b\Big(\delta\boldsymbol{u}^k,q\Big) = -\Big\langle\mathscr{R}_p\left(\boldsymbol{u}^k\right),q\Big\rangle_{\mathbb{Q}',\mathbb{Q}}, \qquad (15)\\
&\frac{1}{\Delta t}g\left(\delta\mathbf{T}_s^k,\boldsymbol{\tau}\right) + \alpha\left(\delta\mathbf{T}_s^k,\boldsymbol{\tau};\boldsymbol{u}^k\right) + \beta\left(\delta\boldsymbol{u}^k,\boldsymbol{\tau};\mathbf{T}_s^k\right)\\
&\qquad = -\Big\langle\mathscr{R}_{\boldsymbol{u},\mathbf{T}_s}(\boldsymbol{u}^k,\mathbf{T}_s^k),\boldsymbol{\tau}\Big\rangle_{\mathbb{W},\mathbb{W}'}, \qquad (16)\\
&\frac{1}{\Delta t}h\left(\delta\varphi^k,\psi;1\right) + i\Big(\delta\varphi^k,\psi;\boldsymbol{u}^k\Big) + j\Big(\psi,\delta\boldsymbol{u}^k;\boldsymbol{\nabla}\varphi^k\Big)\\
&\qquad = -\Big\langle\mathscr{R}_\varphi\left(\varphi^k,\boldsymbol{u}^k\right),\psi\Big\rangle_{\mathbb{X}(0)',\mathbb{X}(0)}. \qquad (17)
\end{aligned}$$

for all test functions $\mathbf{v} \in \mathbb{V}(\mathbf{0})$, $q \in \mathbb{Q}$, $\boldsymbol{\tau} \in \mathbb{W}$ and $\psi \in \mathbb{X}(0)$.

Regarding the space discretization by finite elements, a Taylor-Hood finite element is considered for the velocity $\boldsymbol{u}$ and pressure p, while the P_1 Lagrange polynomials are considered

Algorithm 1 Eulerian fluid-membrane interaction coupling

set initial conditions and Newton tolerance ϵ
from the known values $\boldsymbol{\chi}^{n-1}$
for $t = (n-1)\Delta t, \ldots, T$ **do**
  set initial increment $\left(\delta \boldsymbol{u}_0^n, \delta p_0^n, \delta \mathbf{T}_{s,0}^n\right) = (\mathbf{0}, 0, \mathbf{0})$
  initialize Newton residual $\epsilon_k = 2\epsilon$
  set, from the known values, $p_0^n = p_k^{n-1}$
  initialize the velocity $\boldsymbol{u}_0^n$, tensor $\mathbf{T}_{s,0}^n$ and level set φ_0^n by a second order extrapolated prediction.
  for $k = 1, \ldots$ **do**
    assemble the Jacobian $D\mathscr{R}$ from (14-15-16-17)
    evaluate the residual $\mathscr{R}\left(\boldsymbol{\chi}_k^n\right)$ from (10-11-12-13)
    compute $\delta \boldsymbol{\chi}_n^k$ from (8)
    update $\boldsymbol{\chi}_k^n$ from (9)
    compute Newton residual $\epsilon_{k+1} \equiv \left\|\mathcal{R}_{\boldsymbol{\chi}}\left(\boldsymbol{\chi}^k\right)\right\|$
    if $\varepsilon_k < \epsilon$ **then**
      break
    end if
  end for
  update solution $\boldsymbol{\chi}^n = \boldsymbol{\chi}_{k+1}^n$
  update $\boldsymbol{u}^{n-1} \leftarrow \boldsymbol{u}^n$, $\mathbf{T}_s^{n-1} \leftarrow \mathbf{T}_s^n$, $\varphi_{n-1} \leftarrow \varphi_n$
end for

for the approximation of both tensor $\mathbf{T}_s$ and level set φ. The fluid-membrane interaction coupling method is summarized in Algorithm 1.

IV. Numerical Results and Performance

A. Dynamics of an Oscillating Elastic Membrane

In this example, we present some numerical results for an immersed elastic membrane undergoing an oscillating movement in a surrounding viscous fluid. We follow the test case described in [35]. A stretched pressurized membrane is placed at the center of a square cavity $[-1.5, 1.5] \times [-1.5, 1.5]$.Homogeneous Dirichlet boundary conditions are prescribed for the velocity field, i.e. $\boldsymbol{u}_b = \mathbf{0}$ and $\Sigma_D = \partial\Lambda$. We consider a linear stress-strain law such that

$$\mathcal{W}'(J_s) = \kappa(J_s - 1),$$

where κ represents a constant tension coefficient, see [35]. We set $\kappa = 9$ in our simulations. The fluid is initially stationary. We consider the fluid density $\rho = 1$ and the dynamic viscosity $\mu = 0.015$. The membrane has an ellipsoidal shape at $t = 0$ with major and minor axes 0.75 and 0.5, respectively. Indeed, the membrane is initially stretched and the stretching is equal to 1.2625. Remark that the unstretched configuration corresponds to a circle having the radius $r = 0.5$. Due to the restoring elastic force, the membrane oscillates with gradually smaller oscillations until reaching a circular steady state having the same enclosed area as the initial ellipse.

We perform simulations on a regular mesh generated using the software Gmsh [9] and having $h = 1/100$. We provide in Fig. 2 snapshots showing the oscillating elastic membrane and the velocity field during the first period. Results are in good qualitative agreement with those in [35]. In addition, Fig. 3 shows the temporal evolution of the major and minor axes of the membrane. We clearly see the relaxation of the membrane to the stable circular shape having the radius $r = \sqrt{0.75 \times 0.5} \approx 0.6128$.

B. Convergence Properties of the Newton Strategy

We now proceed with the study of the convergence properties of the Newton method, and we observe the convergence behavior for several values of the time step size. In fact, by increasing Δt, the expected solution becomes far from the starting values of the algorithm (i.e. the second order extrapolation of the solutions at previous time steps). That influences the performance of the method.

We plot in Fig. 4 the convergence curves of the residuals in the semi-logarithmic scale for several time steps. We report the orders of convergence, referred to as ROC, of the residuals in Table I. The ROC is computed as:

$$\text{ROC} = \frac{\ln\left(\dfrac{|\mathscr{R}\left(\boldsymbol{\chi}_k^n\right)|_{\mathbb{V}'(\mathbf{0})}}{|\mathscr{R}\left(\boldsymbol{\chi}_{k-1}^n\right)|_{\mathbb{V}'(\mathbf{0})}}\right)}{\ln\left(\dfrac{|\mathscr{R}\left(\boldsymbol{\chi}_{k-1}^n\right)|_{\mathbb{V}'(\mathbf{0})}}{|\mathscr{R}\left(\boldsymbol{\chi}_{k-2}^n\right)|_{\mathbb{V}'(\mathbf{0})}}\right)}, \qquad \text{for } k > 2.$$

Fig. 4 shows that the convergence of the algorithm is very fast, always less that 10 iterations. From Table I, we observe that the method features a quadratic convergence behavior as expected from a theoretical point of view. Nevertheless, we remark that the number of iterations required for convergence increases when using too large values of Δt. Remark that for large Δt, the convergence is first difficult to reach and the residuals decrease slowly, while approaching the expected second-order behavior beyond a certain threshold value. That results from the local convergence property of the Newton method, and the convergence is deteriorated when the initial guess is not close enough to the solution. In the literature, several strategies enable to address this issue, such as the damped Newton method. That is, however, beyond the scope of the present work.

C. Computational Convergence Study

We now perform a grid convergence study. We perform fully Eulerian simulations of an oscillating pressurized membrane immersed in a viscous fluid, and we use the same setup described above. We study the spatial accuracy of the numerical approximation by computing the normalized errors in several norms on successively refined meshes. The errors are computed with respect to a reference solution obtained with the finest mesh size $h = 1/160$ (referred to by a tilde symbol). Let $\|\cdot\|_{0,2,\Lambda}$ and $\|\cdot\|_{1,2,\Lambda}$ design the L^2-norm and the semi-norm H^1, respectively. The errors are computed at the same time $T = 5$ and are given by:

$$e(\boldsymbol{u}) = \frac{\|\boldsymbol{u}_h - \tilde{\boldsymbol{u}}|_{1,2,\Lambda}}{\|\tilde{\boldsymbol{u}}\|_{1,2,\Lambda}}, \quad e(\mathbf{T}_s) := \frac{\|\mathbf{T}_{s,h} - \tilde{\mathbf{T}}_s\|_{(L^2(\Gamma))^{d\times d}}}{\|\tilde{\mathbf{T}}_s\|_{(L^2(\Gamma))^{d\times d}}},$$

$$e(p) = \frac{\|p_h - \tilde{p}\|_{0,2,\Lambda}}{\|\tilde{p}\|_{0,2,\Lambda}} \text{ and } e(\varphi) = \frac{\|\mathscr{H}_\varepsilon(\varphi_h) - \mathscr{H}_\varepsilon(\tilde{\varphi})\|_{0,2,\Lambda}}{\|\mathscr{H}_\varepsilon(\tilde{\varphi})\|_{0,2,\Lambda}}.$$

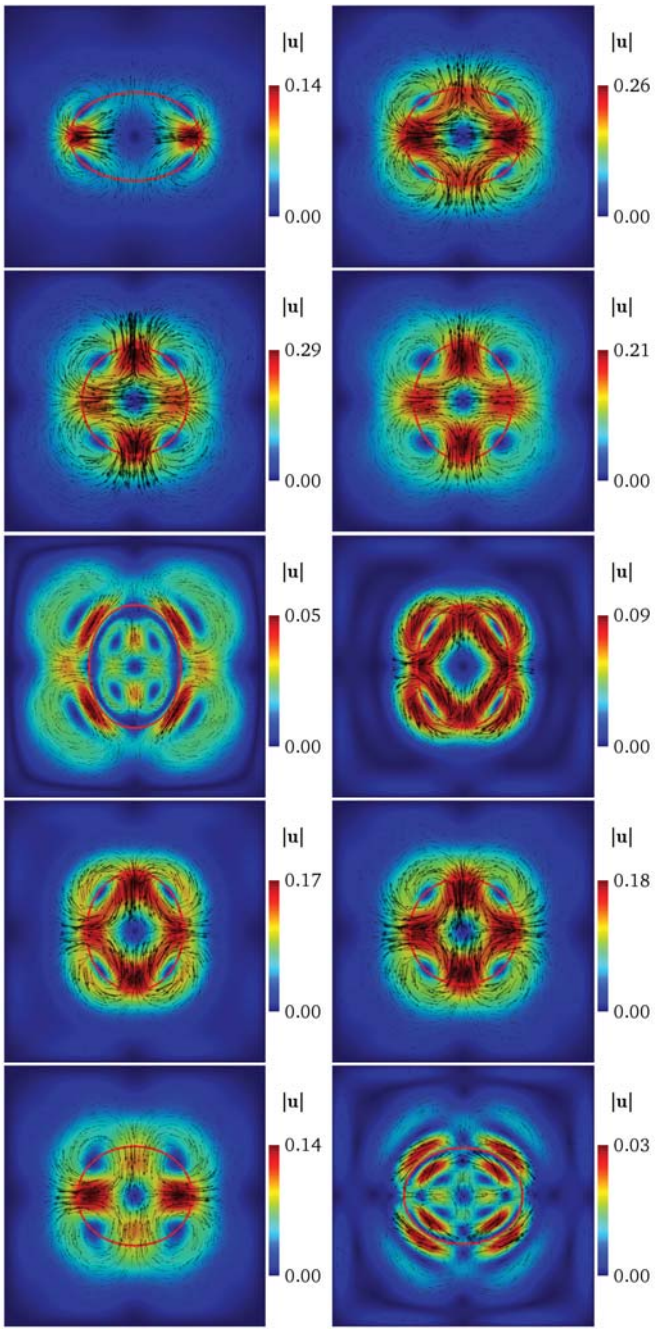

Fig. 2 Snapshots showing the dynamics of the elastic membrane in a viscous flow (shape and velocity profile) at successive times $t \in \{0.1, 0.48, 0.78, 1, 1.38, 1.6, 1.8, 2.2, 2.5, 2.84\}$, respectively from top to bottom and from left to right: Γ is plotted with a continuous red line

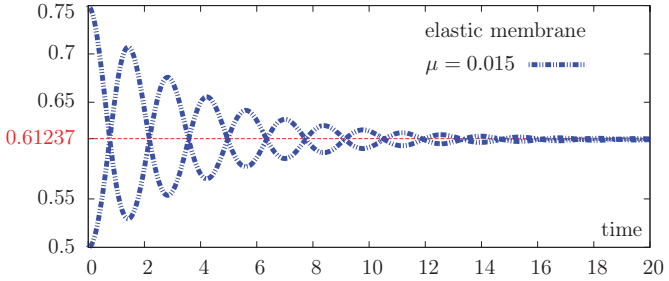

Fig. 3 Temporal evolution of the major and minor axes of the elastic stretched membrane for $\mu = 0.015$

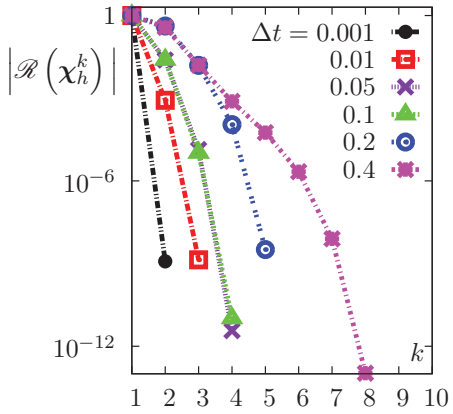

Fig. 4 Convergence curves of the residuals with respect to the Newton iteratios for various time step sizes: Results are plotted in the semi-logarithmic scale

We also evaluate the rate of convergence ROC with respect to the corresponding refinement level, referred to as a superscript l, as:

$$\text{ROC} = \frac{\ln\left(\frac{E^{l-1}}{E^l}\right)}{\ln\left(\frac{h^{l-1}}{h^l}\right)}.$$

The computed errors are reported in Table II, along with the corresponding rates of convergence. The time steps are small enough to avoid significantly influencing the accuracy. Results show that suboptimal convergence rates are obtained for the errors in velocity $\boldsymbol{u}$ and pressure p, whereas $e(\varphi)$ converges with almost a linear convergence behavior. The error in the membrane tension has a convergence behavior of about 0.8.

TABLE I
ORDERS OF CONVERGENCE OF THE RESIDUALS FOR VARIOUS VALUES OF THE TIME STEP

k	$\Delta t = 10^{-3}$	10^{-2}	5×10^{-2}	0.1	0.2	0.4
3	–	1.8810	2.0141	2.0936	3.7611	3.1352
4			2.0229	1.7789	1.5019	0.8045
5					2.1102	1.2234
6						1.2565
7						1.7121
8						2.0023

TABLE II
SPATIAL CONVERGENCE IN THE NATURAL NORMS FOR A PRESSURIZED ELASTIC MEMBRANE IMMERSED IN A FLUID

$1/h$	$e(\boldsymbol{u})$	ROC$_{\boldsymbol{u}}$	$e(p)$	ROC$_p$
20	7.790E-1		5.125E-1	
40	3.795E-1	1.037	2.028E-1	1.337
80	1.928E-2	0.977	9.784E-2	1.051

$1/h$	$e(\mathbf{T}_s)$	ROC$_{\mathbf{T}_s}$	$e(\varphi)$	ROC$_\varphi$
20	9.855E-1		9.355E-2	
40	5.581E-1	0.820	4.887E-2	0.937
80	3.249E-1	0.780	2.572E-2	0.926

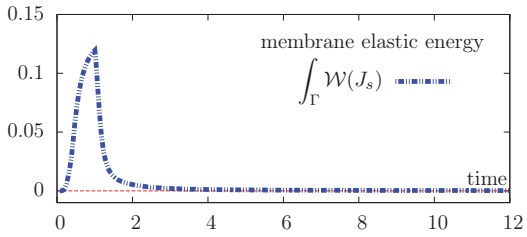

Fig. 5 Temporal evolution of the membrane elastic energy

D. Three-Dimensional Test Case

We now investigate the applicability of the present method in the three-dimensional case. To that aim, we consider a test case in which the elastic membrane is first gradually squeezed under the effect of an external force. Beyond a certain time, the external force vanishes and the membrane is released. Such a membrane squeezing and releasing dynamics can be found in several physical and biological applications, for instance, the GTP-dependant hydrolysis of membranes during endocytosis [4]. There are many industrial applications including the mechanical squeezing of high elastic membranes, such as the industrial filtration process using membrane chamber plates [34]. The fluid is initially at rest and we set the density and viscosity to $\rho = 1$ and $\mu = 0.5$, respectively. The time step size is $\Delta t = 2\times10^{-2}$. We simulate the dynamics of the elastic membrane in the time interval $(0, 12)$. The external squeezing force is given by

$$\boldsymbol{g}(\boldsymbol{x}) = \begin{cases} 4\mathscr{H}_\varepsilon\left(x^2+y^2-0.3\right)\operatorname{sgn}_\varepsilon(z)\delta_\varepsilon(\varphi)z & \text{if } t \leqslant 1, \\ 0, & \text{otherwise.} \end{cases}$$

where $\boldsymbol{x} = (x, y, z) \in \mathbb{R}^3$ denotes the position.

Snapshots in Fig. 6 show the dynamics of the elastic membrane. After releasing the membrane, the shape is relaxed and deforms gradually until reaching the unstretched spherical configuration, where the velocity vanishes. We plot in Fig. 5 the temporal evolution of the membrane elastic energy:

$$\int_\Gamma \mathcal{W}(J_s),$$

showing the energy peak at $t = 1$ when the maximum loading force holds. The elastic energy decreases after the release until reaching zero.

TABLE III
EVALUATION OF THE MAXIMUM TIME STEP Δt_{MAX} ALLOWED BY THE PRESENT METHOD AND THE EXPLICIT METHOD FOR VARIOUS VALUES OF THE MESH SIZE

h	Δt_{max}(Fully implicit)	Δt_{max}(Explicit)
$1/20$	0.41	2.1×10^{-2}
$1/40$	0.16	7.3×10^{-3}
$1/80$	7.4×10^{-2}	2.4×10^{-3}
$1/160$	2.9×10^{-2}	7.2×10^{-4}

E. Comparison with an Explicit Decoupling Scheme

We finally perform a comparative study with a fully explicit decoupling scheme, usually used in the published literature. The explicit scheme consists in decoupling and solving the fluid problem, the level set equation and the advection of the surface tensor in a segregated manner. We first compute the velocity and pressure by solving the fluid problem, in which the elastic force appears as a source term evaluated using the membrane position and the strain invariant at the previous time step. The level set function and the surface tensor are subsequently advected with the computed velocity field. We measure in Table III the maximum time step size allowed by the explicit and implicit methods. Results show that the present method has a significant stabilizing effect and allows to use significantly larger time steps, up to 40 times larger, compared to those allowed by the explicit method. The theoretical investigations of the stability conditions are beyond the scope of this work.

V. CONCLUSION

In the present paper, we have introduced a fully implicit and purely Eulerian finite element method for the numerical modeling of highly deformable membranes immersed in a Newtonian fluid. The method is based on the use of the Newton-Raphson method and a monolithic solver has been implemented. We have considered a simplified characterization of the mechanical properties of the membrane, in which the elastic response is restricted to the surface stretching. A consistent linearization has been performed and an exact Jacobian matrix has been derived. The quadratic convergence of the Newton method has been numerically obtained. In addition, the method has been compared to the standard fully explicit method, showing the robustness of the present approach. The numerical stability has been maintained for significantly larger time steps.

This work represents a first step towards modeling the full mechanical response of elastic membranes. Some extensions of the approach presented in this paper are being currently explored. We are focusing on the development of a cubically convergent Newton variant that would allow significant computational savings. In addition, further investigations of the performance of the present method when using more complex constitutive laws are part of our current work. We also foresee the applicability of the present framework to model the dynamics of highly deformable leaflets of heart valves.

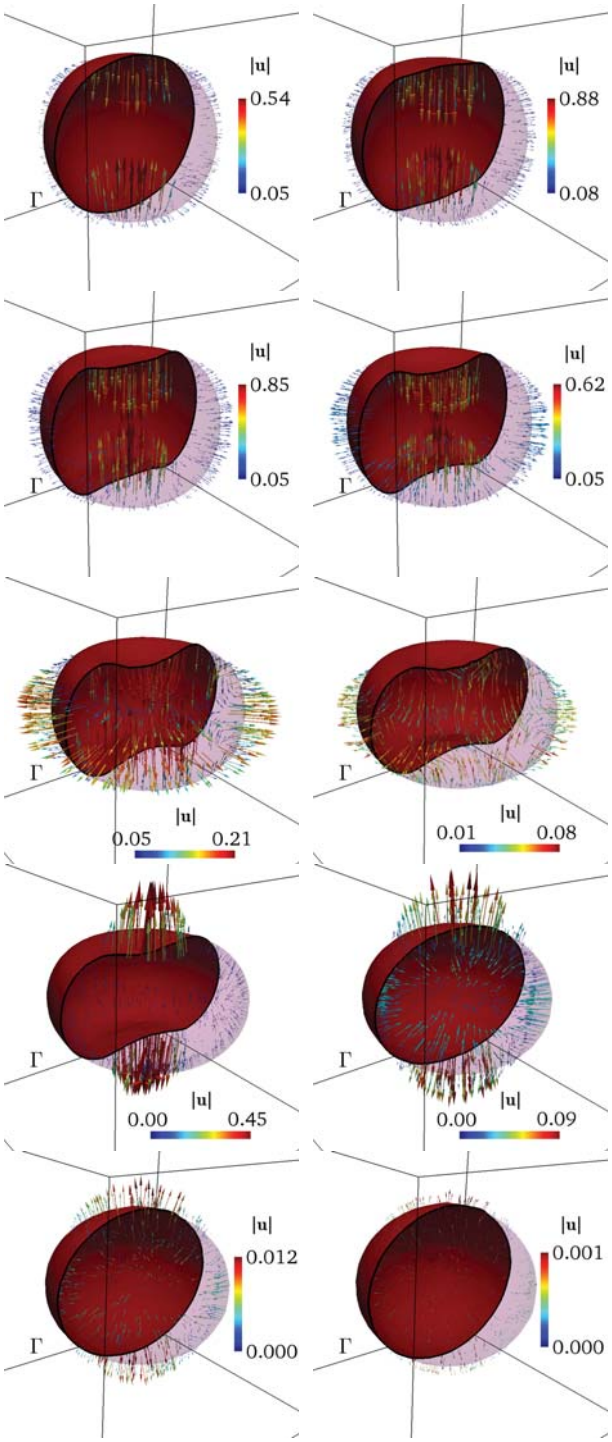

Fig. 6 Snapshots showing the relaxation of an elastic membrane in a viscous flow at successive times $t \in \{0.06, 0.18, 0.3, 0.4, 0.6, 0.9, 1.32, 1.5, 2, 4.18\}$, respectively from left to right and from top to bottom: The figures show the velocity field on the membrane Γ (red color)

APPENDIX
USEFUL DERIVATIVES AND LINEARIZATION EXPRESSIONS

In this Appendix, we provide the directional derivatives of the main problem quantities in the direction of the increment $\delta\boldsymbol{\chi} \equiv (\delta\boldsymbol{u}, \delta p, \delta\mathbf{T}_s, \delta\varphi)$. We have:

$$D\boldsymbol{\nabla}\varphi[\delta\varphi] = \boldsymbol{\nabla}\delta\varphi, \quad D|\boldsymbol{\nabla}\varphi|[\delta\varphi] = \boldsymbol{\nabla}\delta\varphi\cdot\mathbf{n},$$
$$\text{and} \quad D\frac{1}{|\boldsymbol{\nabla}\varphi|}[\delta\varphi] = -\frac{\mathbf{n}\cdot\boldsymbol{\nabla}\delta\varphi}{|\boldsymbol{\nabla}\varphi|^2}$$

yielding the following expression for the linearization of the normal vector:

$$D\mathbf{n}[\delta\varphi] = \frac{\boldsymbol{\nabla}\delta\varphi}{|\boldsymbol{\nabla}\varphi|} - \frac{(\boldsymbol{\nabla}\varphi\cdot\boldsymbol{\nabla}\delta\varphi)\boldsymbol{\nabla}\varphi}{|\boldsymbol{\nabla}\varphi|^3} = \frac{\boldsymbol{\nabla}_s\delta\varphi}{|\boldsymbol{\nabla}\varphi|}.$$

The linearization of the surface projector reads:

$$D\boldsymbol{\pi}_\Gamma[\delta\varphi] = \frac{-1}{|\boldsymbol{\nabla}\varphi|^2}\Big(\boldsymbol{\nabla}_s\delta\varphi\otimes\boldsymbol{\nabla}\varphi + \boldsymbol{\nabla}\varphi\otimes\boldsymbol{\nabla}_s\delta\varphi\Big).$$

For a test function $\mathbf{v}$, that leads to:

$$D\,\mathrm{div}_s\,\mathbf{v}[\delta\varphi] = D\boldsymbol{\pi}_\Gamma[\delta\varphi] : \boldsymbol{\nabla}\mathbf{v}.$$

The linearization of the surface stretching J_s reads:

$$DJ_s[\delta\boldsymbol{\chi}] = DJ_s[\delta\varphi] + DJ_s[\delta\mathbf{T}_s]. \tag{18}$$

We first show that:

$$\begin{aligned} &D\,\mathrm{tr}\,(\mathbf{B}_s)\,[\delta\boldsymbol{\chi}] \\ &\quad = D\mathbf{B}_s : \mathbf{I}[\delta\boldsymbol{\chi}] = D\mathbf{T}_s : \boldsymbol{\pi}_\Gamma[\delta\boldsymbol{\chi}] \\ &\quad = D\,\mathrm{tr}\,\mathbf{B}_s[\delta\mathbf{T}_s] + D\,\mathrm{tr}\,\mathbf{B}_s[\delta\varphi] \\ &\quad = \delta\mathbf{T}_s : \boldsymbol{\pi}_\Gamma - \left(\boldsymbol{\nabla}_s\delta\varphi\otimes\frac{\boldsymbol{\nabla}\varphi}{|\boldsymbol{\nabla}\varphi|^2} + \frac{\boldsymbol{\nabla}\varphi}{|\boldsymbol{\nabla}\varphi|^2}\otimes\boldsymbol{\nabla}_s\delta\varphi\right) : \mathbf{T}_s. \end{aligned}$$

Analogously,

$$\mathrm{tr}\left(\mathbf{B}_s^2\right) = (\mathbf{T}_s\boldsymbol{\pi}_\Gamma) : (\boldsymbol{\pi}_\Gamma\mathbf{T}_s) = (\mathbf{T}_s\boldsymbol{\pi}_\Gamma)^2 : \mathbf{I}.$$

We compute $D\,\mathrm{tr}\left(\mathbf{B}_s^2\right)[\delta\boldsymbol{\chi}]$ following:

$$D\,\mathrm{tr}\left(\mathbf{B}_s^2\right)[\delta\boldsymbol{\chi}] = D\,\mathrm{tr}\left(\mathbf{B}_s^2\right)[\delta\mathbf{T}_s] + D\,\mathrm{tr}\left(\mathbf{B}_s^2\right)[\delta\varphi].$$

We can express the surface stretching as:

$$J_s = \sqrt{\frac{1}{2}\Big((\mathbf{T}_s : \boldsymbol{\pi}_\Gamma)^2 - (\mathbf{T}_s\boldsymbol{\pi}_\Gamma)^2 : \mathbf{I}\Big)}.$$

We end with:

$$DJ_s[\delta\mathbf{T}_s] = \frac{1}{2J_s}\Big((\mathbf{T}_s : \boldsymbol{\pi}_\Gamma)\mathbf{I} - \mathbf{T}_s\boldsymbol{\pi}_\Gamma\Big)\delta\mathbf{T}_s : \boldsymbol{\pi}_\Gamma.$$

The remaining term in the linearization of the strain invariant J_s (18) reads:

$$\begin{aligned} DJ_s[\delta\varphi] &= \frac{1}{4J_s}\,D\Big((\mathbf{T}_s : \boldsymbol{\pi}_\Gamma)^2 - (\mathbf{T}_s\boldsymbol{\pi}_\Gamma)^2 : \mathbf{I}\Big)[\delta\varphi] \\ &= \frac{1}{2J_s}\Big(\mathrm{tr}\,(\mathbf{B}_s)\;\mathbf{T}_s : D\boldsymbol{\pi}_\Gamma[\delta\varphi] - \mathbf{T}_s\boldsymbol{\pi}_\Gamma\mathbf{T}_s : D\boldsymbol{\pi}_\Gamma[\delta\varphi]\Big) \\ &= \frac{1}{2|\boldsymbol{\nabla}\varphi|^2 J_s}\Big(\\ &\qquad \mathbf{T}_s\boldsymbol{\pi}_\Gamma\mathbf{T}_s : \big(\boldsymbol{\nabla}_s\delta\varphi\otimes\boldsymbol{\nabla}\varphi + \boldsymbol{\nabla}\varphi\otimes\boldsymbol{\nabla}_s\delta\varphi\big) \\ &\qquad - \big(\mathbf{T}_s : \boldsymbol{\pi}_\Gamma\big)\big(\mathbf{T}_s : (\boldsymbol{\nabla}_s\delta\varphi\otimes\boldsymbol{\nabla}\varphi + \boldsymbol{\nabla}\varphi\otimes\boldsymbol{\nabla}_s\delta\varphi)\big)\Big). \end{aligned}$$

Finally, the full expression of $DJ_s[\delta\boldsymbol{\chi}]$ is obtained using (18).

ACKNOWLEDGMENT

The authors gratefully acknowledge the financial support by the Swiss National Science Foundation through the grant **320030-149567**.

REFERENCES

[1] P.R. Amestoy and I.S. Duff and J. Koster and J.-Y. L'Excellent, *A Fully Asynchronous Multifrontal Solver Using Distributed Dynamic Scheduling*, SIAM J. Matrix Anal. Appl., 2001, 23(1):15-41.

[2] J.W. Barrett, H. Garcke and R. Nürnberg, *Finite element approximation for the dynamics of asymmetric fluidic biomembranes*, preprint No. 03/2015, University Regensburg, Germany (2015).

[3] D. Barthès-Biesel, *Motion and Deformation of Elastic Capsules and Vesicles in Flow*, Annual Review of Fluid Mechanics, 48 (2016), pp. 25–52

[4] P.V. Bashkirov, S.A. Akimov, A.I. Evseev, S.L. Schmid, J. Zimmerberg and V.A. Frolov, {*GTPase*} *Cycle of Dynamin Is Coupled to Membrane Squeeze and Release, Leading to Spontaneous Fission*, Cell, 135 (7) (2008), pp. 1276–1286

[5] A. Beck, M.J. Thubrikar and F. Robicsek, *Stress analysis of the aortic valve with and without the sinuses of valsalva*, J. Heart Valve Dis., 10(1) (2001), pp. 1–11

[6] F. Brezzi and M. Fortin, *Mixed and hybrid finite element methods*, Springer New York, 15 (1991).

[7] G.-H. Cottet and E. Maitre, *A level-set formulation of immersed boundary methods for fluid-structure interaction problems*, C. R. Acad. Sci. Paris, 338 (7) (2004), pp. 581–586

[8] H. Gao, X. Ma, N. Qi, C. Berry, B.E. Griffith, and X. Luo, A Finite Strain *Nonlinear Human Mitral Valve Model with Fluid Structure Interaction*, Int. J. Numer. Method. Biomed. Eng. 30 (2014), pp. 1597–1613.

[9] C. Geuzaine and J.-F. Remacle, *Gmsh: A 3-D finite element mesh generator with built-in pre- and post-processing facilities*, Int. J. Numer. Meth. Engng., 2009, 79: 1309-1331.

[10] B.E. Griffith, *Immersed boundary model of aortic heart valve dynamics with physiological driving and loading conditions*, Int. J. Numer. Methods Biomed. Engrg. 28(3) (2011), pp. 317–345.

[11] J. de Hart, G.W.M. Peters, P.J.G. Schreurs, and F.P.T. Baaijens, *A three-dimensional computational analysis of fluid–structure interaction in the aortic valve*, J. Biomech. 36(1) (2003), pp. 103–112.

[12] M.E. Gurtin and A.I. Murdoch *A continuum theory of elastic material surfaces*, Arch. Ration. Mech. Anal. 57 (4) (1975), pp. 291–323

[13] I.C. Howard, E.A. Patterson, and A. Yoxall, *On the opening mechanism of the aortic valve: some observations from simulations*, J. Med. Engrg. Tech. 27 (2003), pp. 259–266.

[14] S. Hysing, *A new implicit surface tension implementation for interfacial flows*, Int. J. Numer. Methods Fluids, 51 (6) (2006), pp. 659–672

[15] Y. Kim and M.-C. Lai, *Simulating the dynamics of inextensible vesicles by the penalty immersed boundary method*, J. Comput. Phys., 229 (12) (2010), pp. 4840–4853

[16] A. Laadhari, R. Ruiz-Baier and A. Quarteroni, *Fully Eulerian finite element approximation of a fluid-structure interaction problem in cardiac cells*, Int. J. Numer. Meth. Engng. 96 (2013) 712–738.

[17] A. Laadhari and G. Székely, *Eulerian finite element method for the numerical modeling of fluid dynamics of natural and pathological aortic valves*, J. Comput. Appl. Math., Accepted 2016, doi: 10.1016/j.cam.2016.11.042.

[18] A. Laadhari and A. Quarteroni, *Numerical modeling of heart valves using resistive Eulerian surfaces*, Int. J. Numer. Method. Biomed. Eng. 32 (5) (2016)

[19] A. Laadhari, P. Saramito, and C. Misbah, *An adaptive finite element method for the modeling of the equilibrium of red blood cells*, Int. J. Numer. Meth. Fluids 80 (2016) 397–428.

[20] A. Laadhari, P. Saramito, and C. Misbah, *Computing the dynamics of biomembranes by combining conservative level set and adaptive finite element methods*, J. Comput. Phys. 263 (2014) 328–352.

[21] M-C. Lai and C.S. Peskin, *An Immersed Boundary Method with Formal Second-Order Accuracy and Reduced Numerical Viscosity*, J. Comput. Phys. 160 (2) (2000), pp. 705–719

[22] X.Z. Li, D. Barthes-Biesel and A. Helmy, *Large deformations and burst of a capsule freely suspended in an elongational flow*, J. Fluid Mech. 1988; 187(2):179–196.

[23] M.P.I. Forum, *MPI: A Message-Passing Interface Standard*, http://www.mpi-forum.org (Accessed: 28.11.2016).

[24] MUMPS: MUltifrontal Massively Parallel Solver, http://mumps.enseeiht.fr/index.php (Accessed: 28.11.2016).

[25] S. Osher and J.A. Sethian *Fronts propagating with curvature-dependent speed: Algorithms based on Hamilton-Jacobi formulations*, J. Comput. Phys., 79 (1) (1988), pp. 12–49

[26] Paraview: Parallel visualization application, http://paraview.org (Accessed: 28.11.2016).

[27] C. Pozrikidis and S. Ramanujan *Deformation of liquid capsules enclosed by elastic membranes in simple shear flow: large deformations and the effect of fluid viscosities*, J. Fluid Mech 361 (4) (1998), pp. 117–143

[28] A. Quarteroni, R. Sacco and F. Saleri, *Numerical Mathematics*, Springer-Verlag, New York, 37, 2000.

[29] A. Rahimian and S. K. Veerapaneni and G. Biros *Dynamic simulation of locally inextensible vesicles suspended in an arbitrary two-dimensional domain, a boundary integral method*, J. Comput. Phys., 229 (18) (2010), pp. 6466–6484

[30] P. Saramito, *Efficient C++ finite element computing with Rheolef*, CNRS-CCSD ed., 2013. http://www-ljk.imag.fr/membres/Pierre.Saramito/rheolef/rheolef-refman.pdf (Accessed: 22.09.16).

[31] D. Salac and M. Miksis, *A level set projection model of lipid vesicles in general flows*, J. Comput. Phys., 230 (2011), pp. 8192–8215

[32] U. Seifert, *Configurations of fluid membranes and vesicles*, Adv. Phys. 46 (1997) 13–137.

[33] Y. Seol, W.-F. Hu, Y. Kim and M.-C. Lai, *An immersed boundary method for simulating vesicle dynamics in three dimensions*, Preprint (2016)

[34] H.J. Spölgen, *Membrane for a membrane plate for a plate filter press*, *EP Patent App. EP19,970,113,291*, Google Patents 11 (1998), www.google.fr/patents/EP0827766A1?cl=en (Accessed: 29.11.2016).

[35] Z. Tan and D.V. Le and Zhilin Li and K.M. Lim and B.C. Khoo *An immersed interface method for solving incompressible viscous flows with piecewise constant viscosity across a moving elastic membrane*, J. Comput. Phys. 227 (23) (2008), pp. 9955–9983

[36] T. Williams and C. Kelley, *Gnuplot: An Interactive Plotting Program*, http://www.gnuplot.info (Accessed: 28.11.2016).

Aymen Laadhari received the Engineering degree from Tunisia Polytechnic School, Tunisia, in 2006. He received the Ph.D. degree in Applied Mathematics from Grenoble University, France, in 2011. He was a scientific collaborator with the Mathematics Institute of Computational Science and Engineering at the École Polytechnique Fédérale de Lausanne (Swiss Federal Institute of Technology Lausanne), Switzerland. He is currently a researcher with the Swiss Federal Institute of Technology Zürich, Switzerland. His current research interests include mathematical modeling and software development of new computational methods for the simulation of biomedical phenomena.

Gábor Székely is currently a Prof. em. Dr. with the Swiss Federal Institute of Technology Zürich, Switzerland. He has been working at ETH Zurich since 1997, and as a full professor since 2008. His research focuses on medical image analysis, a field in which he has conducted pioneering work on the automatic recognition of organs in CT and MRI data. This has resulted in substantial contributions to the computer-assisted planning and implementation of surgical interventions. With other driving forces, he has developed his Computer Vision Laboratory into one of the leading global centres for training surgeons using virtual reality simulation methods.